Int. J. Heat Mass Transfer. Vol. 29, No. 4, pp. 593–610, 1986
Printed in Great Britain

0017–9310/86 $3.00 + 0.00

Numerical simulation of buoyant, turbulent flow—II. Free and mixed convection in a heated cavity

J. A. C. HUMPHREY and W. M. TO
Department of Mechanical Engineering, University of California, Berkeley, CA 94720, U.S.A.

(*Received* 4 *February* 1985 *and in final form* 30 *October* 1985)

Abstract—In Part I of this study two models were developed for predicting free and mixed convection low Reynolds number turbulent flows. Detailed comparisons between measurements and predictions for the case of free convection along a heated, vertical, flat plate showed that both models yield accurate results for the mean flow and heat transfer. As a result, the simpler of the two (a k–ε formulation based on the notion of eddy diffusivities for momentum and heat) was extended to predict steady free and mixed convection flows of air in a strongly heated cavity of arbitrary rectangular cross-section and orientation. This is the subject of the present communication.

Numerical calculations show that the details of free convection flow in a heated cavity are strongly governed by the characteristics of the local heat transfer. The characteristics depend on the cavity aspect ratio, a/b, the inclination angle, α, and the Grashof number, Gr_b. For example, stable stratification of heated fluid inside a tilted cavity strongly dampens the turbulent fluctuations, thus reducing convective heat losses from the cavity. Calculations performed for the free convection cases investigated experimentally by Humphrey *et al.* [Sandia Report No. SAND 84–8192 (1985); *Phil. Trans. R. Soc.* **A316**, 57–84, (1985)] show good qualitative agreement with measurements of the velocity and temperature distributions. Predictions of the Nusselt number, Nu_b, display trends which are also in accord with the measurements. For mixed convection, the details of the flow become asymptotically independent of α as the ratio of inertia to buoyant forces, characterized by Re_b^2/Gr_b, is increased. For $a/b = 1$ and $\alpha = 45°$, predictions reveal a minimum in Nu_b when $Re_b^2/Gr_b \sim 1$. Many of the complex flow patterns revealed experimentally, for both free and mixed convection, are reproduced numerically.

1. INTRODUCTION

1.1. *The problem of interest and objective of this study*

CONSIDER a two-dimensional, partial enclosure such as the one of square cross-section shown in Fig. 1, the interior surfaces of which are heated to a temperature T_w above that of the environment which is at T_∞. This configuration is here referred to as a 'heated cavity'. It arises frequently in systems of engineering interest including solar cavity receivers, the ventilation of rooms and corridors, fire and smoke propagation through buildings and the cooling of electronic components.

In the absence of an externally imposed flow, buoyant forces will induce fluid motion within the cavity. The nature and intensity of this motion will depend on the cavity cross-section, a/b, its orientation, α, a characteristic Grashof number for the flow, $Gr_b = g\beta_\infty \Delta T b^3/\nu_\infty^2$, and the overheat ratio, $\Delta T/T_\infty = (T_w - T_\infty)/T_\infty$. The Grashof number determines whether the flow will be laminar or turbulent, and the oveheat ratio determines whether a constant or variable physical properties condition applies. If $\Delta T/T_\infty$ is small, then the Boussinesq approximation can be assumed [1].

In the presence of an externally imposed flow, of speed u_∞ and of angle ϕ with respect to the cavity aperture plane, inertial forces compete against the buoyancy for control of the flow. The Reynolds number, $Re_b = u_\infty b/\nu_\infty$, now becomes an important parameter, and this 'mixed' convection regime is characterized by the ratio Re_b^2/Gr_b, a relative measure of inertial to buoyant forces in the flow.

This study concerns the numerical calculation of fully elliptic, turbulent, steady and two-dimensional (in the mean) flows in strongly heated cavities of rectangular cross-section for arbitrary values of α, ϕ, a/b, Re_b^2/Gr_b and $\Delta T/T_\infty$. The fluid medium is air for which the Prandtl number is $Pr = 0.71$. Because the basic element of a heated cavity is the flat plate, this configuration is also of special interest.

The accurate calculation of free convection flow along a heated, flat plate is considered to be a logical first step towards the accurate numerical simulation of heated cavity flows. Part I of this work was devoted to this problem. Two models of turbulence were developed for predicting the characteristics of free convection flow along a heated, vertical, flat plate. Both models are variable-property, low Reynolds number formulations which dispense with *a priori* prescriptions of near-wall relations for velocity and temperature. Instead numerical calculations are performed on refined grids, well into the viscous sublayer region of the flow. One formulation, the KEM, is based on the notion of spatially dependent, isotropic eddy diffusivities for the turbulent transport of momentum and heat. The second, the ASM, obtains the turbulent fluxes directly from a system of algebraic equations derived by neglecting the convective and diffusive transport of these fluxes in their respective conservation equations. There are no limitations in the models which preclude their application to mixed convection flows.

NOMENCLATURE

a cavity width
A_0 area of cavity aperture plane
b cavity height
c length of the cavity normal to x–y plane
C_p specific heat at constant pressure
C_μ constant in equation (3)
D turbulence quantity related to ε through ν, $\overline{(\partial u_i'/\partial x_j)(\partial u_i'/\partial x_j)} = \varepsilon/\nu$
g gravitational constant
g_i component i of the gravitation vector
G buoyancy production of turbulent kinetic energy, $\overline{\rho' u_i'} g_i$
Gr_b cavity Grashof number (with $\Delta T = T_c - T_\infty$), $g\beta_\infty \Delta T b^3/\nu_\infty^2$
h cavity heat transfer coefficient (based on aperture area)
k turbulent kinetic energy, $\overline{u_i' u_i'}/2$
l length scale of energy-containing eddies, equation (6)
n coordinate direction perpendicular to a surface
Nu_b cavity Nusselt number, equation (9), hb/γ_∞
Nu' alternative definition of the cavity Nusselt number, equation (10)
p pressure
Pr Prandtl number, $\mu C_p/\gamma$
Pr_t turbulent Prandtl number
$\dot{Q}_{ap}$ heat transfer through cavity aperture plane
$\dot{Q}_w$ total heat transfer from cavity walls
$\dot{q}_w$ wall heat flux
R gas constant for air
Re_b cavity Reynolds number, $u_\infty b/\nu_\infty$
St cavity Stanton number, $h/(\rho_\infty C_p u_\infty)$
T temperature
T_c arithmetic average of the three cavity wall temperatures
T_∞ ambient temperature (293 K)
u velocity component in x-direction
u_i velocity component in i-direction
u_τ characteristic shear stress velocity, $\sqrt{\tau_w/\rho}$
u_∞ velocity of wind approaching a cavity
v velocity component in y-direction
x coordinate direction, defined in Fig. 1
y coordinate direction, defined in Fig. 1
y^+ dimensionless coordinate, y/y_τ
y_τ wall-region length scale, ν/u_τ

Greek symbols
α cavity inclination angle, defined in Fig. 1
β coefficient of volume expansion, $1/T_\infty$
γ thermal conductivity
δ boundary-layer thickness
ΔT characteristic temperature difference, $T_w - T_\infty$; taken as $T_c - T_\infty$ in a cavity
ε isotropic dissipation of turbulent kinetic energy, νD
η_T inner region length scale, equation (5), $[(\nu_\infty/Pr)^2/(g\beta_\infty \Delta T)]^{1/3}$
θ nondimensional temperature, $(T - T_\infty)/(T_c - T_\infty)$
μ molecular viscosity
μ_t turbulent viscosity
ν molecular kinematic viscosity
ρ density
σ_ϕ turbulent Prandtl number for scalar ϕ
τ_w wall shear stress
ϕ arbitrary scalar quantity; also orientation of wind approaching a cavity.

Superscripts
$'$ fluctuating quantities
$\bar{}$ mean quantities.

Subscripts
i,j spatial indices
t turbulent quantity
w wall condition
∞ ambient condition.

Detailed comparisons between measurements and predictions presented in Part I of this study show clearly that the algebraic stress model (ASM) is capable of resolving correctly the anisotropic characteristics of turbulent free convection along heated, flat plates. However, this model is only marginally superior to the k–ε model (KEM) when consideration is restricted to a prediction of the mean flow and heat transfer. As a result, it was decided to extend and apply the simpler KEM formulation to simulate free and mixed convection flows in strongly heated cavities of arbitrary rectangular cross-section and orientation. This is the subject of the present communication.

1.2. *Free and mixed convection in the cavity configuration*

The following is a summary of those studies reviewed by Humphrey *et al.* [2, 3] most meaningful to the present work.

Motivated by an interest in fire and smoke spread problems, Ku *et al.* [4], Markatos *et al.* [5], and Kumar and Cox [6] have applied high Reynolds number forms of the k–ε turbulence model to predict two-dimensional, buoyancy-driven flows in cavity-related configurations. *Ad hoc* extensions to the low Reynolds number k–ε model of Jones and Launder [7] have been formulated by Fraikin *et al.* [8] and Sagara [9], but

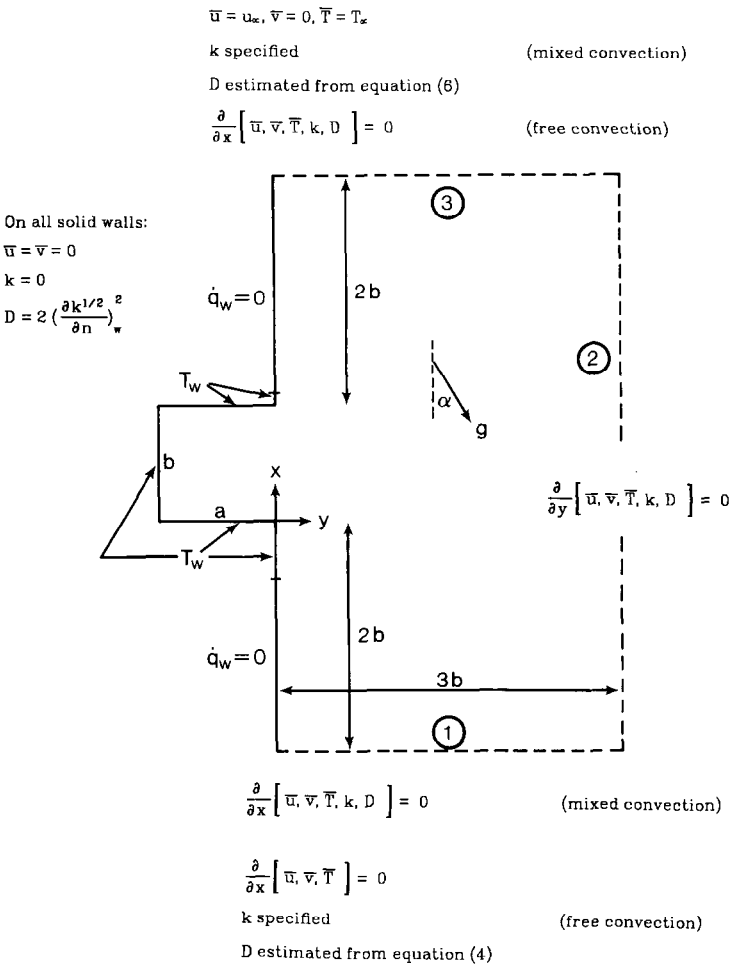

FIG. 1. Boundary conditions for a heated cavity in free or mixed convection regimes. For mixed convection, the upper and lower edges of the cavity are *completely* adiabatic.

they have been applied only to fully enclosed, rectangular configurations. All of the above studies invoke the Boussinesq approximation thus limiting the results to low overheat ratios. It appears that numerical models have not been extensively developed for predicting free and mixed convection turbulent flows in cavities of arbitrary orientation.

The corresponding state of experimentation is equally incomplete. Hess and Henze [10] have performed experiments using flow visualization and the laser–Doppler velocimeter (LDV) technique in a three-dimensional cavity at relatively low values of $\Delta T/T_\infty$. Only the back wall of their cavity was heated. The use of water as the fluid medium allowed them to attain Rayleigh numbers ranging from 2×10^{10} to 2×10^{11}. They observed that the flow became turbulent at a Rayleigh number of about 7×10^{10}. However, the data in ref. [2] suggests that this transition value can be considerably lower when heating (with its attendant destabilization effects) is applied to upward facing horizontal or inclined walls.

In consecutive investigations, Penot [11] and Mirenayat [12] have studied the free convection of air in a cubical cavity with all five walls equally heated to overheat ratios ranging from 0.04 to 0.47. Flow visualization and limited velocity measurements using the LDV technique were performed. However, very extensive heat transfer measurements were made as a function of Grashof number and cavity orientation from which Mirenayat [12] derived the following Nusselt number correlation based on the aperture plane area:

$$Nu_b = a_1 Gr_b^{a_2} \quad (10^7 < Gr_b < 4 \times 10^9) \qquad (1)$$

where Gr_b is the cavity Grashof number as defined in the Nomenclature. In equation (1), a_1 and a_2 are parameters which depend on the cavity inclination angle, α; b is the cube side. Typically, $0.15 < a_1 < 0.60$ and $0.30 < a_2 < 0.37$, strongly supporting a 1/3 power dependence on Gr_b. Kraabel [13] has also investigated the free convection of air in a cubical cavity with all five walls heated. The large characteristic dimension of the

cavity (2.2 m) permitted obtaining values of Gr_b as large as 1.2×10^{12} for overheat ratios ranging between 0.39 and 2.55 approximately. Measurements in the aperture plane were used to determine the air temperature, velocity, enthalpy flux and radiation heat flux distributions. Convective heat losses from the cavity were derived from these data. The aperture plane Nusselt number correlation obtained by Kraabel [13] is:

$$Nu_b = 0.44\, Gr_b^{1/3}(T_w/T_\infty)^{0.18} \quad (10^7 < Gr_b < 1.2 \times 10^{12}). \tag{2}$$

This correlation is valid only for the inclination angle $\alpha = 0°$, but it is in very good agreement with Mirenayat's [12] lower overheat ratio results for which $a_1 = 0.465$ and $a_2 = 0.33$ when $\alpha = 0°$. One of the main conclusions to be drawn from the measurements in refs. [12] and [13] is the length scale independence of the cavity convective heat transfer coefficient. Measurements and calculations of the heat transfer coefficient for turbulent free convection along a vertical flat plate, discussed in Part I of this work, also show this length scale independence.

Humphrey *et al.* [2, 3] have performed a detailed experimental study of the turbulent flow and heat transfer in a two-dimensional, rectangular cavity with $\Delta T/T_\infty = 1.26$ and $Gr_b = 4.4 \times 10^7$ for various values of the cavity aspect ratio and orientation. LDV measurements of the velocity and turbulent stress components were obtained for the free convection regime. Measurements of temperature and extensive flow visualization were performed for both the free and mixed convection regimes. The numerical simulation of their experimental observations has been the primary objective of the present work.

2. TURBULENCE MODEL AND NUMERICAL PROCEDURE

The turbulence model used for the present calculations is the variable physical property KEM closure described in detail in Part I of this study. In this closure the turbulent flux of any fluctuating scalar quantity ϕ (u_i, T, k, etc.) is related to the spatial gradient of the corresponding mean quantity, Φ, via a spatially dependent eddy diffusion coefficient. In this generalization of the Boussinesq assumption the eddy diffusion coefficient for ϕ given by

$$\frac{\mu_t}{\sigma_\phi} = C_\mu \frac{\bar{\rho} k^2}{\sigma_\phi \varepsilon} \tag{3}$$

where it is tacitly assumed that $k^{1/2}$ and $k^{3/2}/\varepsilon$ are proportional to the turbulent velocity and length scales, respectively. In equation (3), σ_ϕ is the turbulent Prandtl number for the quantity ϕ and, like C_μ, it is a model constant. (All the KEM model constants are given in Part I of this work.)

Because the fluid medium is air, a perfect gas equation of state is used to relate variations in density to variations in temperature. A simple relation for the mean square of the temperature fluctuations, $\overline{T'^2}$, is derived from its transport equation under the assumption of an equilibrium flow.

Empirical wall relations for velocity and temperature are deliberately avoided in the formulation. Instead, the low Reynolds number approximation initially proposed by Jones and Launder [7] is extended and improved. As explained in detail in Part I of this work, in this approach numerical calculations are performed all the way into the viscous sublayer region of the flow. Damping of the turbulent fluctuations near walls is simulated by requiring that the turbulent viscosity vary according to a Van Driest-type relation.

Finite-difference forms of the elliptic transport equations for momentum, energy, turbulent kinetic energy and its rate of dissipation are solved on a 2-D nonuniform grid using an under-relaxed iteration technique that is implicit in time. The solution procedure is the REBUFFS code developed by LeQuere *et al.* [14], extended to include the KEM formulation as described in Part I of this work. No special difficulties were experienced in obtaining steady-state, grid-independent results for the conditions investigated.

2.1. *Boundary conditions*

The solution of the system of elliptic equations describing the flow in a heated cavity requires a specification of appropriate boundary conditions for the unknown variables along the boundaries of the calculation domain. Figure 1 shows the conditions used for the free and mixed convection calculations, respectively.

(i) *Solid walls.* The specification of wall conditions for velocity and temperature in earlier studies of natural convection in heated cavities (and enclosures) have been inconsistent and sometimes vague; contrast, for example [5, 8, 9]. Sagara [9] does not explain clearly how the wall region is treated. Law-of-the-wall relations were tacitly assumed by Markatos *et al.* [5]. In spite of the fact that Fraikin *et al.* [8] pursue a low Reynolds number approach, looking at the way the boundary value for dissipation was imposed, it appears that the first calculation node was placed in the inertial flow region. In all three studies it is unclear how the wall condition for temperature was dealt with. As pointed out in Part I of this work, even in pure free convection there are no universally applicable power-law relations for velocity and temperature, since the general dependence on temperature and surface orientation of the coefficients in such relations is simply unknown.

Wall boundary conditions in the present cavity calculations were prescribed in the same way as for the flat plate, described in Part I of this work. The procedure requires specifying the value of the turbulent kinetic energy at the wall. The dissipation condition, together with no slip, impermeable wall conditions for velocity and the wall temperature (known from the

experiments) are summarized below:

$$\bar{u}_i = 0$$
$$\bar{T} = T_w$$
$$k = 0 \tag{4}$$
$$D = 2\left(\frac{\partial k^{1/2}}{\partial n}\right)_w^2$$

where T_w denotes a constant value or a prescribed variation of wall temperature, and n denotes the coordinate direction normal to the wall in question. For the free convection calculations, the following values for T_w measured by Humphrey *et al.* [2, 3] were imposed along the inside walls of the heated cavity: $T_{top} = 611$ K, $T_{back} = 673$ K, $T_{bottom} = 673$ K. In the experiments these values did not change significantly with a/b or α. Similarly, the temperature distributions measured along the upper and lower heated edges of the cavity were imposed. For the parametric mixed convection calculations, all walls inside the cavity were fixed to $T_w = 643$ K, the entire upper and lower edges being assumed adiabatic.

An estimate of the thickness of the viscous sublayer region is needed to maintain the necessary grid refinement in the numerical claculations. For free convection this is derived from the flat plate correlation obtained by George and Capp [15] who find

$$1.7 \approx \frac{y}{\eta_T} = y^+ \frac{y_\tau}{\eta_T}. \tag{5}$$

In Part I of this work it is shown that y^+ is approximately 4. During the course of calculation the grid refinement is continuously checked against this criterion.

(ii) *The far field (free boundaries).*

(*a*) *Free convection.* An accurate way of specifying far field boundary values for velocity, based on the analysis of the flow induced by a heated point source, has been described by LeQuere *et al.* [14] in relation to predicting laminar free convection flow in a heated cavity. It was shown in ref. [14] that, while a realistic calculation of the far field flow pattern does require careful attention to the specification of the far field boundary conditions, the characteristics of the flow inside and immediately in front of a cavity do not differ significantly from those calculated by simply specifying zero normal gradients of velocity everywhere along the far field boundaries. Since the free convection cases investigated in refs. [2, 3] are the ones of concern to this study, boundary conditions were implemented which are in closest accord with those experimental observations. Thus, for pure free convection, zero normal gradients for $\bar{u}$, $\bar{v}$ and $\bar{T}$ were specified on all three free boundaries. A small value of turbulent kinetic energy was specified by setting $k = 0.007\ m^2\ s^{-2}$ on the upstream free boundary (boundary '1' in Fig. 1). The value of D on this boundary was estimated by means of equation (4). On the other two free boundaries the normal gradients of k and D were set to zero. The condition for sufficiently small gradients of the variables on the free boundaries was guaranteed by determining appropriate positions for the latter through a trial and error procedure. Further discussion concerning the accuracy of this approach is provided in Section 3.2, subsection (ii).

(*b*) *Mixed convection.* In contrast to the free convection case, far field mixed convection boundary conditions were not determined in the experiment of refs. [2, 3] and it was necessary to approximate these. A uniform flow at ambient temperature was specified on the upsteam free boundary (boundary '3' in Fig. 1). As for free convection, a small value of k was specified on this boundary by setting $k = 0.007\ m^2\ s^{-2}$. The value of D was not calculated from equation (4). Instead, it was estimated from the inviscid approximation [16]

$$\varepsilon = vD \approx A\frac{k^{3/2}}{l} \tag{6}$$

in which the values of A and l were set to 1 and $0.01b$, respectively. Zero normal gradients were prescribed for all variables on the other two free boundaries.

2.2. *Testing and grid refinement*

Besides the heated cavity results presented and discussed in the next section, additional tests were performed to: (a) validate various purely numerical aspects of the calculation procedure; and (b) check the performance of the KEM model for two limiting flow conditions (free convection along a heated flat plate and forced convection in a heated cavity). Purely numerical aspects were checked by reproducing some of the heated cavity laminar flow cases reported in LeQuere *et al.* [14], and the limited free convection velocity measurements of Sernas and Kyriakides [17]; and by calculating the time-dependent characteristics of 2-D and 3-D wall-driven laminar flows in an enclosure with and without an initially imposed, stable stratification. Results for the latter tests, reported in Koseff *et al.* [18], show that the 2-D calculations are in very good agreement with the measurements and predictions of others, but that the 3-D calculations are prone to numerical diffusion. Calculations pertaining to turbulent free convection along a heated, flat plate have already been presented and discussed extensively in Part I of this work. Predictions of forced convection in a heated cavity, corresponding to the experiment of Fox [19] and the mixing length calculation by Chin *et al.* [20], are provided in Humphrey *et al.* [21], where good agreement is reported with respect to the data available for velocity and temperature.

The outcome of this extensive testing is the conclusion that, subject to the grid distribution considerations discussed below, the results of the next section are essentially free of any serious numerical inaccuracy so that significant discrepancies arising between measurements and calculations must be explained in terms of experimental and/or turbulence model uncertainties.

Numerical explorations showed that an unevenly spaced grid composed of 69 × 53 nodes (in the x- and y-directions, respectively) was sufficient to yield grid-independent cavity flow calculations. Of these nodes, 31 × 31 were contained in the cavity with not less than five nodes always located within the respective wall viscous sublayers. A factor of 1.3 was used for expanding the grid from each wall in the cavity. With this scheme about six nodes ended up between the wall and the position of maximum velocity along each wall. All calculations were performed on the CDC 7600 machine at the Lawrence Berkeley Laboratory. Typically, 490K octal words of computer storage and 750 iterations (1.1 s per iteration) were needed to obtain converged results. The criterion for convergence is explained in Part I of this work. For the cavity calculations the additional condition was imposed that the total heat flow from the cavity walls should equal that through the aperture plane to within 1%.

3. RESULTS AND DISCUSSION

3.1. *Preliminary considerations*

The KEM formulation presented in Part I of this work is extended here to retain direct buoyancy contributions to the balances of turbulent kinetic energy and dissipation [the terms represented by G and $C_{\varepsilon 3}GD/k$ in equations (13) and (14) in Part I]. The quantity $\overline{\rho' u_i'}$ in the buoyancy production of k, $G = \overline{\rho' u_i'} g_i$, was modeled by combining equations (6) and (9) in Part I to yield the following gradient approximation:

$$\overline{\rho' u_i'} g_i = \frac{1}{T} \frac{\mu_t}{Pr_t} \frac{\partial \bar{T}}{\partial x_i} g_i. \tag{7}$$

It was pointed out in Part I that the application of equation (7) to heated, vertical, flat plates leads to a physically inconsistent contribution to the balance of k. However, it was also shown that the error incurred through doing this is small, due to the dominance of the shearing production of k. By contrast, equation (7) does provide a physically consistent approximation for the buoyant production of k along heated, horizontal and inclined, flat walls. Calculations discussed below show that in the heated cavity configuration, regardless of orientation, extensive portions of the flow have a large component of the temperature gradient aligned with the direction of gravity. As a consequence, (7) is expected to provide a useful approximation for the calculation of G in the k and ε equations.

Values for the constant $C_{\varepsilon 3}$ in the buoyancy term in the dissipation equation have been determined for isolated vertical ($C_{\varepsilon 3} = 1.44$) and horizontal ($C_{\varepsilon 3} = 0.288$) walls by Rodi [22]. The correct value for a wall of arbitrary orientation is not known. In their studies, involving the flows in a heated cavity and an enclosure, respectively, Markatos *et al.* [5] and Sagara [9] neglect the buoyant contribution to dissipation altogether ($C_{\varepsilon 3} = 0$). By contrast, Fraikin *et al.* [8] use $C_{\varepsilon 3} = 0.7$ in their enclosure calculations. None of these studies involved inclined walls. Lacking further knowledge concerning an appropriate value for $C_{\varepsilon 3}$ for the walls in a cavity of arbitrary orientation, three values (0.7, 0.9, 1.1) were tested. The value 0.9 is roughly the average of the values for isolated vertical and isolated horizontal walls. The values 0.7 and 1.1 were used to explore the effects on the flow of inducing a relative decrease and increase respectively in the buoyant contribution to dissipation. Turbulence quantities (such as k and ε) and the heat transfer were found to decrease with increasing values of $C_{\varepsilon 3}$, but the effects on mean velocity and temperature were relatively minor. The cavity Nusselt number computed using $C_{\varepsilon 3} = 0.7$ was 8.3% larger than the value computed using $C_{\varepsilon 3} = 1.1$. Of the values tested, $C_{\varepsilon 3} = 0.7$ provided the most consistent overall agreement with the quantities measured by Humphrey *et al.* [2, 3] on the aperture plane of their cavity. This was the value used in the present calculations.

The next two subsections present results and discussions of KEM predictions of free and mixed convection flows in heated cavities. The free convection calculations correspond to the experimental conditions investigated by Humphrey *et al.* [2, 3] in which $Gr_b = 4.4 \times 10^7$ and $\Delta T/T_\infty = 1.26$ with: $a/b = 1$, $\alpha = 0°$; $a/b = 1$, $\alpha = 45°$; and $a/b = 0.5$, $\alpha = 0°$. An investigation of the influence of the parameters a/b, α and ΔT on cavity Nusselt number is also presented. Mixed convection flow has been computed only for the case $a/b = 1$, $\alpha = 45°$; but varying the free-stream velocity such that $Re_b^2/Gr_b = 0.4$, 0.85, 21.3 and 85.4, respectively.

3.2. *Free convection*

The structure of the flow inside a heated cavity depends strongly on the cavity orientation and aspect ratio. The size and intensity of the recirculating flow region induced at the lower corner of the aperture plane depends primarily on the inclination angle, α, of the cavity. However, for shallow cavities ($a/b < 1$) the reattachment location of the separated flow also depends on the cavity aspect ratio. The stable stratification of heated fluid, and hence the damping of turbulent fluctuations in the cavity, depend on both α and a/b. The combination of these and related complex flow characteristics determines the convective heat loss from the cavity. Following a summary of some general heat transfer results, detailed numerical predictions for the experimental conditions investigated in refs. [2, 3] are examined.

(i) *Heat transfer.* Integration of the energy equation over the rectangular control volume bounded by the three heated cavity walls and the aperture plane yields:

$$C_p \int_{A_0} (\bar{\rho}\bar{v} + \overline{\rho' v'})\bar{T}\, \mathrm{d}A + C_p \int_{A_0} \overline{\rho' T'} \bar{v}\, \mathrm{d}A - \int_{A_0} \left(\gamma + C_p \frac{\mu_t}{Pr_t}\right) \frac{\partial \bar{T}}{\partial y}\, \mathrm{d}A = \dot{Q}_w \tag{8}$$

where A_0 is the area of the cavity aperture and $\dot{Q}_w$ is the total heat conduction from the three heated cavity

walls. The LHS of equation (8) represents the heat transferred through the aperture plane, denoted by $\dot{Q}_{ap}$. (This, as opposed to $\dot{Q}_w$, was the quantity estimated in ref. [2] from the LDV measurements of $\bar{v}$.) The aperture plane Nusselt number is evaluated numerically as,

$$Nu_b = \frac{\dot{Q}_w/c}{\gamma_\infty \Delta T} \tag{9}$$

where c is the length of the cavity normal to the x–y plane, $\Delta T = (T_c - T_\infty)$, and T_c is the average of the three wall temperatures, $T_c = (T_{top} + T_{back} + T_{bottom})/3$.

Table 1 provides a comparison between measurements and predictions of Nu_b for conditions corresponding to the experimental study. Also shown in the table are the Nusselt numbers predicted for the individual walls for each of the cases investigated. The predictions show that the heat transfer from the top wall is always less than from the other two walls for both aspect ratios and orientations. Inclining the cavity significantly decreases the heat transfer from both the top and the back walls, due to the reduction in speed of the fluid along these tilted walls and to the stable stratification of fluid trapped in the cavity. By contrast, the heat transfer from the bottom wall, whose heated surface is tilted facing upward, is slightly increased. The heat transfer from the back wall in the shallow cavity is greater than that from the back walls in the deeper cavities. This is due to the impingement on the back wall of the shallow cavity of *part* of the flow which separates at the bottom inlet corner; a phenomenom which is not observed in cavities with $a/b \geqslant 1$ for which flow reattachment always takes place completely on the bottom wall. As a result it may be concluded that while the total convective heat loss from a shallow cavity can exceed that from a deep cavity, inclining a cavity should always work to reduce the total convective loss.

Although the trends in the predicted aperture plane Nusselt numbers are consistent with the measurements, the absolute values differ significantly. A detailed error analysis in ref. [2] shows that the experimental Nusselt numbers, calculated by assuming

$$\dot{Q}_w = \dot{Q}_{ap} = (\bar{p}/R) C_p \int_{A_0} \bar{v}\, dA$$

in equation (9), are prone to systematic uncertainties which, unfortunately, are difficult to quantify. They arise mainly from nonuniform seeding and weak but significant three-dimensionality in the flow. While these two effects introduce only a small deviation in the individual measurements of velocity, their cumulative effect on the calculation of $\dot{Q}_{ap}$ is potentially serious. It is shown [2] that the resulting uncertainties can account for a systematic *underestimation* of the heat transfer through the cavity aperture plane (by as much as 50% when $a/b = 1$, $\alpha = 0°$). Given the accuracy with which the KEM formulation predicts the mean flow and heat transfer characteristics pertaining to free convection along a vertical, flat plate, and forced convection in a heated cavity, one is tempted to blame the experimental uncertainties for the Nu_b discrepancies shown in Table 1. But caution must be exercised since it will be shown below that, although fairly good predictions are obtained on average for the free convection velocity and temperature distributions in heated cavities, the discrepancies observed in the predictions of these variables can be explained in terms of an *underprediction* of the eddy diffusion coefficient, μ_t. The resultant underprediction of turbulent diffusion of momentum and heat between cold and hot fluid respectively entering and leaving the cavity will lead to an *overprediction* of Nu_b.

Figure 2a shows the dependence of Nu_b on Gr_b for free convection in heated cavities with the same orientation but different aspect ratios. The points, joined by continuous lines in the figure, were calculated by varying the aperture height of the cavity ($b = 0.1, 0.2$ and 0.3 meters) for each aspect ratio. As anticipated from earlier discussion, for a given Grashof number it is seen that the convective heat loss from the shallow cavity is the largest, followed by the square and deep cavities, respectively. A dependence of the Nusselt number on $Gr_b^{0.31}$ is observed for the three aspect ratios, over the range $4.8 \times 10^7 \leqslant Gr_b \leqslant 1.3 \times 10^9$. This result suggests that the cavity heat transfer coefficient, h, is (at most) only a weak function of the characteristic length scale, b. This numerical finding for 2-D cavities is in close agreement with the length scale independence of the heat transfer coefficient observed experimentally in 3-D cavities; see Section 1.2 and [12, 13, 23].

Table 1. Measured and predicted Nusselt numbers for the free convection cavity flow experiment of ref. [2]

		$a/b = 0.5, \alpha = 0°$	$a/b = 1, \alpha = 0°$	$a/b = 1, \alpha = 45°$
Nu_i	top wall	18.87	13.77	4.34
	back wall	23.24	21.15	13.45
	bottom wall	22.89	21.68	22.94
Nu_b	prediction	65.01	56.61	40.71
	measurement	54.1 ± 3.8	27.2 ± 3.2	16.6 ± 3.2

$$Nu_i = \left(\int_0^{l_w} \gamma \frac{\partial \bar{T}}{\partial n}\, dl \right)_i \Big/ \gamma_\infty \Delta T = \frac{\dot{Q}_i/c}{\gamma_\infty \Delta T}$$

where i denotes the wall considered, n is normal to the wall and l is tangent to the wall.

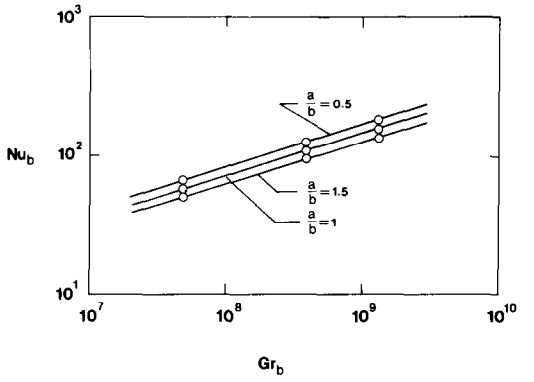

FIG. 2a. Prediction of Nu_b vs Gr_b for free convection flow in a heated cavity: $\alpha = 0°$; $\Delta T/T_\infty = 1.19$; $a/b = 1.5$, 1 and 0.5.

The effect on heat transfer of varying the cavity orientation for conditions corresponding to $a/b = 1$ and a low overheat ratio, $\Delta T/T_\infty = 0.17$, are shown in Fig. 2b. The points joined by dotted lines in the figure are the calculated results. Also shown are the best fits to the experimental measurements of ref. [12] for a heated, cubical cavity at the same two inclination angles. In the figure, the definition for the Nusselt number, Nu', used in ref. [12] is adopted. It is based on the total heated internal surface area, S, and is given by

$$Nu' = \frac{\dot{Q}_w b}{S\gamma_\infty \Delta T}. \tag{10}$$

For a cube $S = 5L^2$ where L is the cube side. Both sets of results in Fig. 2b show that increasing the cavity inclination angle, α, decreases the convective heat losses. As before, both the predictions and measurements support a 1/3 power dependence of Nu' on Gr_b. The agreement between the 2-D calculations and the 3-D measurements of Nu' is unexpected and misleading since it is known [13] that the mean flow emerging from a cubical cavity is strongly three-dimensional and this must influence the heat transfer. Individual wall calculations for the conditions of Fig. 2b [21] confirm this point. The calculated Nu for the top and back walls of the heated 2-D cavity are considerably larger than the values measured for the cube. The smaller rates of heat transfer from these walls in the cube are attributed to the higher characteristic temperature achieved by the air, due to 3-D mixing. The closeness of the results in Fig. 2b must be ascribed to the additional heat transfer from the two side walls in the cubical cavity which renders the surface-averaged losses roughly equivalent.

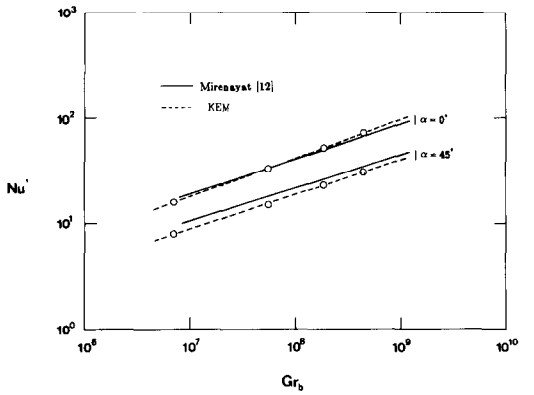

FIG. 2b. Prediction (dotted lines) of Nu' vs Gr_b for free convection flow in a heated cavity: $a/b = 1$, $\Delta T/T_\infty = 0.17$, $\alpha = 0°$ and 45°. Best fits (continuous lines) to the measurements of Mirenayat [12] in a cubical cavity are also shown.

(ii) *Flow characteristics.* Due to space limitations, we have chosen only the case with $a/b = 1$ and $\alpha = 0°$ for detailed examination here. However, where appropriate some of the results for the other two cases investigated ($a/b = 1$, $\alpha = 45°$ and $a/b = 0.5$, $\alpha = 0°$) will also be mentioned. Complete results for all three cases are available in ref. [21].

Plots of the velocity vector fields and of temperature for all three cases are shown in Figs. 3 and 4, respectively. Large regions of recirculating flow arise along the bottom cavity wall when $\alpha = 0°$, and in *all* cases reattachment occurs on the *bottom* wall. For the shallow cavity this produces a striking downward redirection of part of the flow in the shear layer impinging on the back wall. This pattern has been observed in flow visualization experiments [2, 3]. When $\alpha = 0°$ a second (smaller) region of recirculating flow arises downstream of the aperture plane top corner, where the hot air is discharged from the cavity.

Inspection of the figures shows that tilting the cavity forward significantly reduces both the magnitude and extent of the buoyancy-induced motion within the cavity. In spite of the net through-flow, trapped hot air is stably stratified inside the tilted cavity and works to slow down the mean motion and dampen the turbulent fluctuations. Unable to penetrate the stably stratified pool of fluid, air rising along the inclined back wall skirts past it to emerge from the cavity. This shearing motion, combined with a weaker buoyancy driven motion within a thin layer of fluid adjacent to the tilted top wall, induces a weak counter-clockwise recirculation of the hot air in the pool.

Calculations of the turbulent kinetic energy and of the temperature fluctuations (available in ref. [21]) show large values for these quantities along the bottom and back walls of the cavity with $a/b = 1$ and $\alpha = 0°$. In both of these regions the shearing production of k, and hence the production of $\overline{T'^2}$, is large. Along the top wall, stable stratification and wall-damping significantly reduce the levels of k and $\overline{T'^2}$. The highest levels of turbulent kinetic energy arise where the hot air is discharged from the cavity. This is due to shearing production of k as the air turns and accelerates around the top corner. By contrast, large values of $\overline{T'^2}$ are not observed in this region [where $\overline{T'^2} \propto (\partial \bar{T}/\partial y)^2$] because of the strong reduction in $\partial \bar{T}/\partial y$ by turbulent diffusion. The calculations show that large portions of

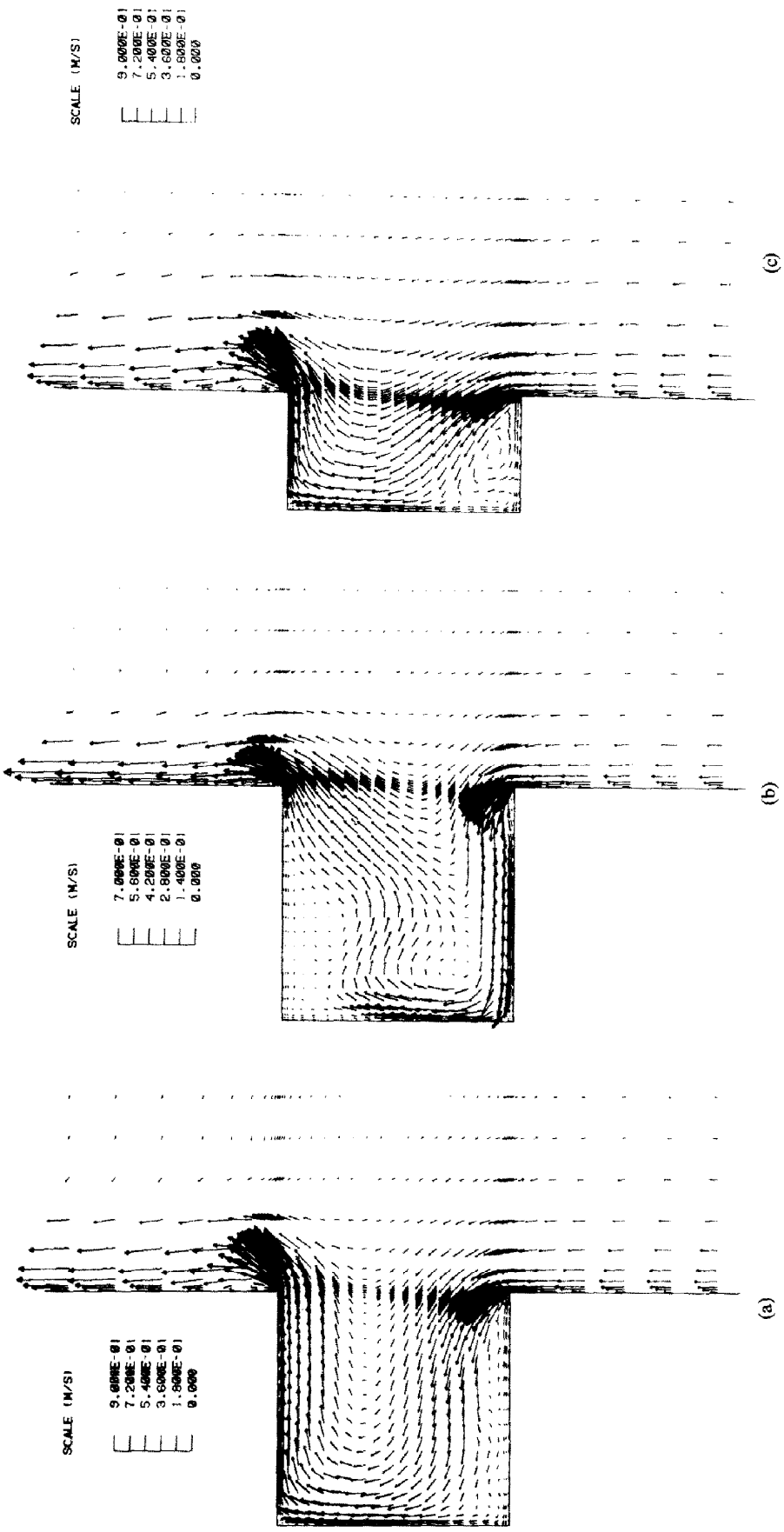

FIG. 3. Velocity vector plot for free convection flow in a heated cavity with $Gr_b = 4.4 \times 10^7$ and $\Delta T/_\infty = 1.26$. From left to right: $a/b = 1, \alpha = 0°$; $a/b = 1, \alpha = 45°$; $a/b = 0.5, \alpha = 0°$.

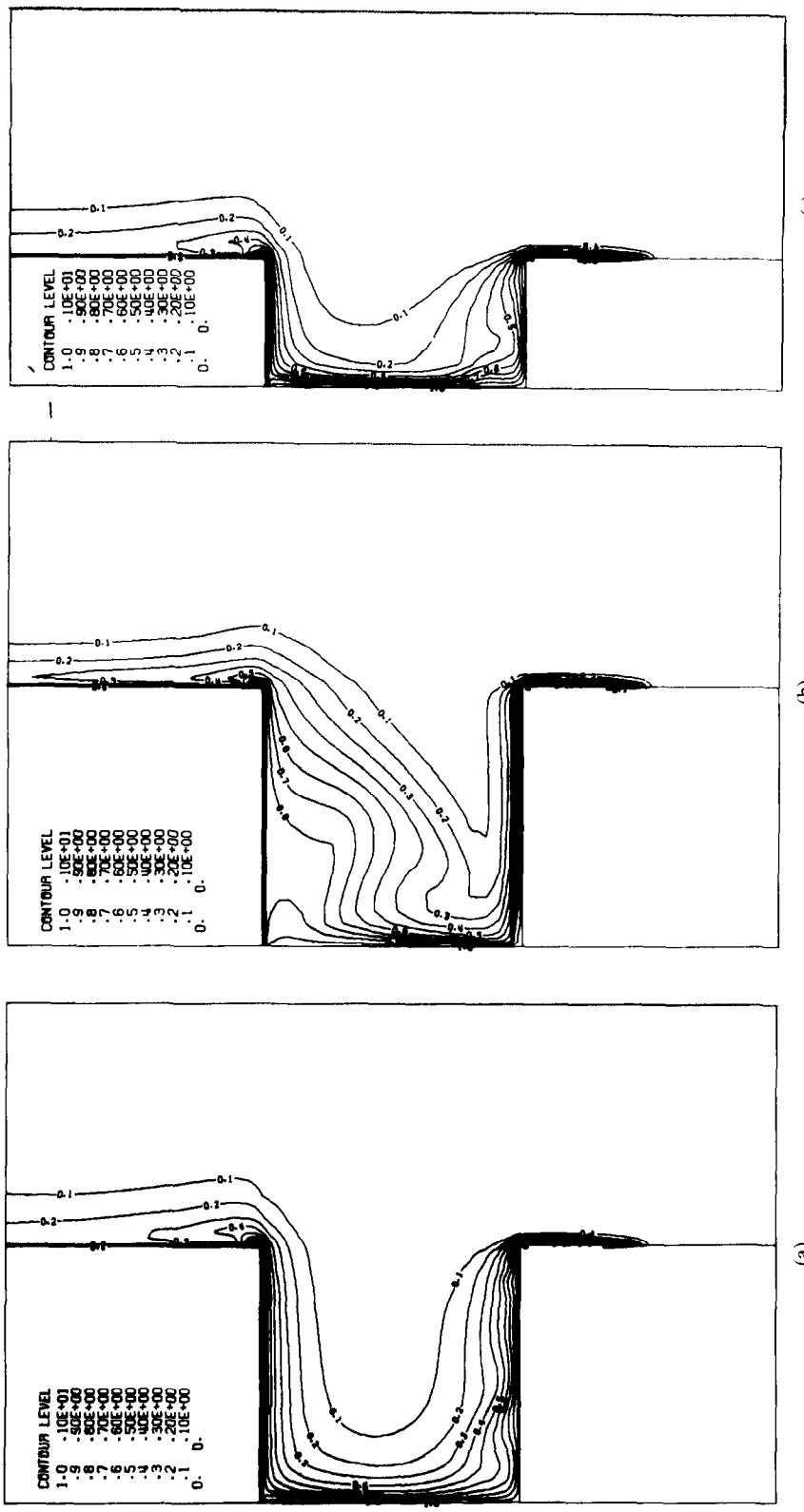

FIG. 4. Contours of nondimensional temperature (θ) for free convection flow in a heated cavity with $Gr_b = 4.4 \times 10^7$ and $\Delta T/T_\infty = 1.26$. From left to right: $a/b = 1$, $\alpha = 0°$; $a/b = 1$, $\alpha = 45°$; $a/b = 0.5$, $\alpha = 0°$.

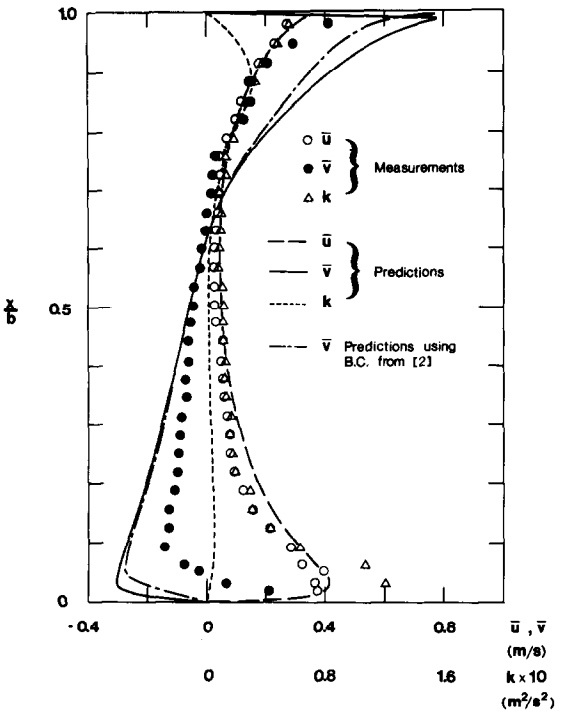

FIG. 5a. Aperture plane profiles of measured (points) and predicted (lines) x- ($\bar{u}$) and y- ($\bar{v}$) components of velocity and turbulent kinetic energy (k) for free convection flow in a heated cavity: $a/b = 1, \alpha = 0°, Gr_b = 4.4 \times 10^7, \Delta T/T_\infty = 1.26$. Experimental data from refs. [2, 3].

the cavity are occupied by essentially turbulence-free air at ambient temperature.

Distributions for k and $\overline{T'^2}$, qualitatively similar to those described above, were obtained in the shallow cavity ($a/b = 0.5$, $\alpha = 0°$). By contrast, stable stratification in the inclined cavity ($a/b = 1, \alpha = 45°$) strongly reduced the extent and magnitude of both quantities. For this case, the turbulent kinetic energy and the temperature fluctuations peaked near the bottom inside corner of the cavity. Large temperature fluctuations were also predicted in the thin fluid layer skirting the pool of hot air trapped in the cavity.

Quantitative comparisons with the measurements [2, 3] for $a/b = 1$ and $\alpha = 0°$ are shown in Figs. 5 and 6. (Plots for the other two cases investigated are available in ref. [21].) Two sets of calculations are provided. One was performed using the far field boundary condition treatment for free convection described in Section 2.1. The other was performed using precisely the experimental values determined in refs. [2, 3] for

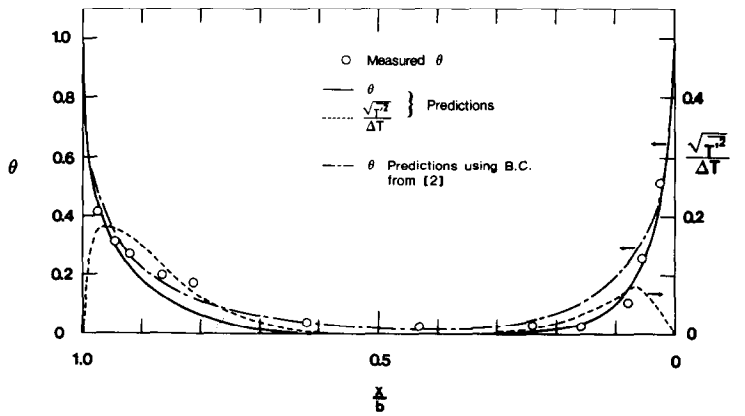

FIG. 5b. Aperture plane profiles of measured (points) and predicted (lines) nondimensional temperature (θ) and predicted (dotted line) normalized temperature fluctuations $[(\overline{T'^2})^{1/2}/\Delta T]$ for free convection flow in a heated cavity: $a/b = 1, \alpha = 0°, Gr_b = 4.4 \times 10^7, \Delta T/T_\infty = 1.26$. Experimental data from refs. [2, 3].

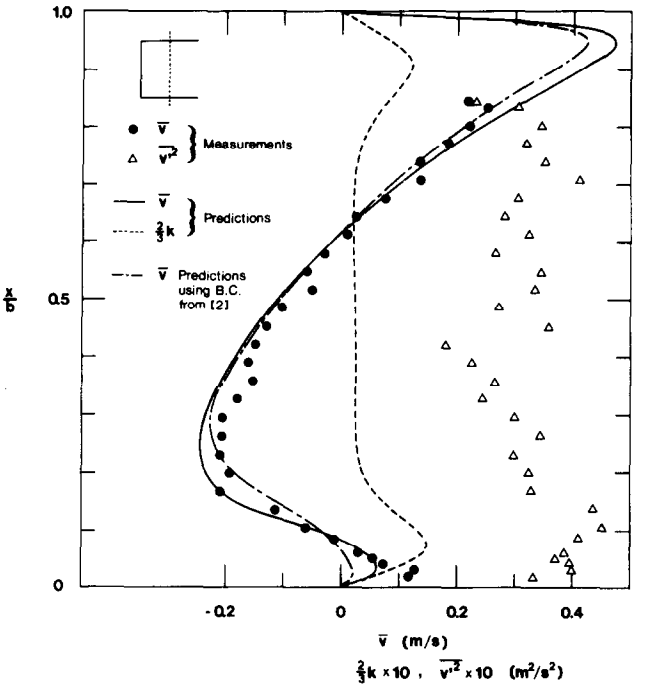

FIG. 6a. Comparisons between: measurements (points) and predictions (lines) of the y- ($\bar{v}$) component of velocity; measurements (points) of $\overline{v'^2}$ and predictions (dotted line) of $2k/3$; for free convection flow in a heated cavity: $a/b = 1$, $\alpha = 0°$, $Gr_b = 4.4 \times 10^7$, $\Delta T/T_\infty = 1.26$. The insert shows the (vertical) comparison location inside the cavity. Experimental data from refs. [2, 3].

$\bar{u}$, $\bar{v}$ and k along a set of free boundaries located considerably *nearer* to the aperture plane. It is seen that the differences are small between the two sets of calculations. This is an important and very useful finding for it implies that the free convection flow and heat transfer characteristics of a heated cavity are strongly determined by local events, the far field having only a minor influence. A similar finding was communicated by LeQuere *et al.* [14] for the case of laminar free convection flow.

The predicted $\bar{u}$ velocity component, on the aperture plane (Fig. 5a) and inside the cavity (Fig. 6b), is in fairly good agreement with the measurements. Similar agreement for this component was obtained for the

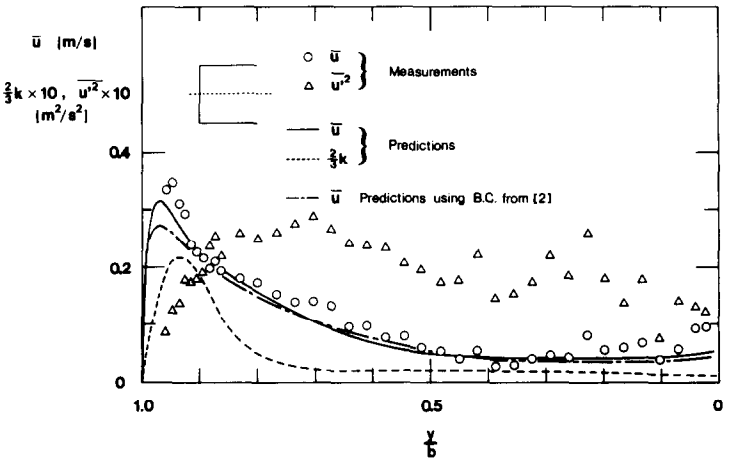

FIG. 6b. Comparison between: measurements (points) and predictions (lines) of the x- ($\bar{u}$) component of velocity; measurements (points) of $\overline{u'^2}$ and predictions (dotted line) of $2k/3$; for free convection flow in a heated cavity: $a/b = 1, \alpha = 0°, Gr_b = 4.4 \times 10^7, \Delta T/T_\infty = 1.26$. The insert shows the (horizontal) comparison location inside the cavity. Experimental data from refs. [2, 3].

other two cases investigated. By contrast, the absolute value of the $\bar{v}$ component (Fig. 5a) is overpredicted along the aperture plane, although there is agreement with regard to the position for $\bar{v} = 0$. A similar result was obtained for $a/b = 0.5$ and $\alpha = 0°$. Calculations of the $\bar{v}$ component for $a/b = 0.5$ and 1 with $\alpha = 0°$ failed to reproduce the region of reversed flow extending through the aperture plane along the bottom wall of the cavity. However, good agreement was obtained inside the cavities (see Fig. 6a for the present case) and along the aperture plane of the cavity with $a/b = 1$ and $\alpha = 45°$. Admitting the possibility of a large (but improbable) positioning error in the measurement aperture plane location when $\alpha = 0°$, we compared calculated $\bar{v}$ profiles at $y/a = -0.02$ with the measurements and found no significant improvements. Given the numerical accuracy of the calculations, particularly in this region of the flow where the grid is especially refined, and the relatively small uncertainty in the measurement of $\bar{v}$, we must point to a failing in the turbulence model to explain the discrepancies observed for $\bar{v}$ in the aperture plane when $\alpha = 0°$.

First, we draw attention to the rather low levels of predicted turbulent kinetic energy and normal stress components (estimated as $2k/3$) respectively shown in Figs. 5a, 6a and 6b. Similar results were obtained in the cavity with $a/b = 0.5$ and $\alpha = 0°$, but *not* in that with $\alpha = 45°$, where stably stratified fluid significantly reduced the level of the fluctuations. Although it is shown [2, 3] that the fluctuating velocity measurements are prone to systematic uncertainties which inflate their value, even a reduction of 65% (an upper limit to the magnitude of all the uncertainties combined) fails to bring the measurements into acceptable conformity with the calculations. Second, we note that larger values of k in equation (3) would imply larger values predicted for the eddy diffusion coefficient, μ_t, and, as a consequence, increased turbulent diffusion. An increase in the turbulent diffusion of momentum between the flows entering and leaving the cavity would bring the aperture plane $\bar{v}$ component and k calculations in closer agreement with the measurements. From this argument we conclude that it seems likely the eddy diffusion coefficient of the mixing motion has been underpredicted. Further considerations suggest why, as well as how this shortcoming might be relieved.

In the relation for μ_t given by equation (3) the quantity C_μ has been fixed to the constant value 0.09. Pourahmadi and Humphrey [24] show that, in fact, C_μ is a complicated function of streamline curvature, the pressure-strain and wall-damping effects. Parallel work by Ljuboja and Rodi [25] shows that the effects of buoyancy will also work their way into a more generalized expression for C_μ, thus yielding larger values for this quantity in unstably stratified flows. The expression derived in ref. [25], for the case of horizontal and vertical buoyant wall jets (parabolic flows) is of the form $C_\mu = (\overline{u'^2}/k)\omega$, where $\overline{u'^2}$ is determined from an algebraic stress model relation and ω is a function of a wall damping function, the buoyant production of $\overline{u'^2}$ and 10 model constants which must be determined experimentally. While a similar but more general relation can be derived for the present elliptic flow, it involves additional undetermined constants. Unfortunately, currently available experimental data bases are not sufficiently extensive or accurate enough to allow an unambiguous optimization of all constants. Even within the context of an algebraic stress formulation (see Part I of this work), for which it is unnecessary to prescribe an eddy diffusion coefficient, μ_t, and hence a function for C_μ, the problem of constant optimization remains. As a result, we have chosen to accept the shortcoming of the present, simpler model, anticipating that the existence of absolute discrepancies between measurements and calculations will not invalidate the relative trends revealed by the calculations. However, we do expect the accuracy of the present KEM formulation to increase as $Re_b^2/Gr_b \to \infty$.

Figure 5b compares measurements and predictions of nondimensional temperature on the aperture plane. (Calculated dimensionless temperature fluctuations are also provided even though measurements are not available.) Agreement is relatively good although the measurements suggest a thicker layer of heated air emerging from the cavity than is actually predicted. This is consistent with the overprediction of $\bar{v}$ near the top of the aperture plane, shown in Fig. 5a; all other conditions being equal, the reduced residence time of a parcel of air in the cavity should lead to a relative reduction of its energy content. The calculations reveal relatively large temperature fluctuations near the top and the bottom corners of the aperture plane, and a fairly uniform flow at ambient temperature crossing the rest of the aperture plane.

3.3. *Mixed convection*

In the experiments of refs. [2, 3] some interesting phenomena and flow structures were observed for heated cavity flows in the mixed convection regime, depending on the relative magnitude of buoyant and inertial forces. The purpose of this part of the numerical study has been to establish the relative effects of an imposed flow on the convective losses from a heated cavity. The flow structure in a heated cavity in the mixed convection was examined for different free-stream velocities such that the parameter of interest, Re_b^2/Gr_b, varied over a meaningful range. In the calculations $\alpha = 45°$, $a/b = 1$ and $u_\infty = 0.7$, 1, 5 and 10 m s^{-1}, corresponding to $Re_b^2/Gr_b = 0.4$, 0.85, 21.3 and 85.4, respectively. The boundary conditions for these calculations have been discussed in Section 2.1.

(i) *Heat transfer.* The variation in Nu_b with Re_b^2/Gr_b is shown in Fig. 7. A minimum Nusselt number occurs at about $Re_b^2/Gr_b = 1$ for which buoyant and inertial forces in the vicinity of the aperture plane are expected to be of comparable magnitude. With some hindsight gained from an inspection of the flow details, discussed below, the minimum in Nu_b is explained as follows. As the free-stream velocity initially increases, hot air

discharged from the cavity is swept downwards in the free-stream direction and partly re-entrained into the cavity. Consequently, the average temperature of stratified air in the cavity is raised, resulting in reduced heat transfer from the cavity walls. Further increases in the free-stream velocity induce a recirculating flow inside the cavity which gradually destroys the stable stratification. Eventually, the flow and heat transfer patterns acquire the characteristics of a shear-driven, forced convection flow with large, turbulent fluxes.

For very small or very large values of the parameter Re_b^2/Gr_b, the expression for the Nusselt number characterizing a heated cavity flow is expected to acquire limiting forms. For large values of Re_b^2/Gr_b one expects an independence of Gr_b. Physically this means that buoyant forces, and hence cavity orientation, are of negligible importance in formulating an expression for Nu_b. A straight line joining the two points calculated for high values of Re_b^2/Gr_b follows the relation,

$$Nu_b = 21.16(Re_b^2/Gr_b)^{0.43}. \tag{11}$$

This expression can be rewritten in terms of a Stanton number by taking $Pr = 0.71$ and $Gr_b = 4.4 \times 10^7$ which were held constant throughout the calculations. The result is

$$St = 0.0154\, Re_b^{-0.14} \tag{12}$$

which is in qualitative agreement with the high Reynolds number semi-empirical correlation obtained by Haugen and Dhanak [26] for forced convection in heated cavities of square cross-section:

$$St = 0.149(\delta/b)^{-0.14}\, Re_b^{-0.25}. \tag{13}$$

To show this we note that, for the conditions of the calculated flow developing along the upper edge of the cavity, a developing length $|x|/b \geqslant 8$ is required before transition to turbulence will occur when $Re_b^2/Gr_b = 85.4$ (the highest value calculated). Thus, for the boundary-layer thickness, δ, in equation (13) we take the laminar flow result $\delta \sim (\nu x/u_\infty)^{1/2}$, and it is straightforward to show that

$$St \approx Re_b^{-0.18}. \tag{14}$$

Since the -0.14 power dependence of δ in equation (13) was derived for turbulent flow, we should not expect a complete correspondence between the Re_b power dependence calculated numerically, equation (12), and that determined experimentally, equation (14).

(ii) *Flow characteristics.* Detailed velocity vector fields, isotherms, turbulent kinetic energy and temperature fluctuation contours for mixed convection are provided in Humphrey *et al.* [21]. The principal observations are presented below with a small sample of the results.

Figures 8 and 9 show the velocity and temperature fields inside a shear-driven cavity at $Re_b^2/Gr_b = 0.85$ and 21.3, respectively. For $Re_b^2/Gr_b < 0.4$ the flow is dominated by buoyant forces, while for $Re_b^2/Gr_b > 2$ it is dominated by inertial forces.

At $Re_b^2/Gr_b = 0.85$ the flow field is still influenced by buoyant forces. (Compare with Fig. 3b for pure free convection.) Hot air leaving the cavity is immediately redirected by the shearing action of the externally imposed flow. Figure 9a shows that some of this hot air is returned to the cavity where the attendant rise in average temperature is the cause for the reduction in heat transfer shown in Fig. 7. In contrast to the pure free convection case (Fig. 3b), at $Re_b^2/Gr_b = 0.85$ *all* the air in the cavity flows in a clockwise direction due to the shear imposed by the external flow. Notwithstanding, velocities are very small in the stratified hot air region.

At $Re_b^2/Gr_b = 21.3$ the flow field shown in Fig. 8b is dominated by inertial effects and loses any tendency to be redirected by buoyancy forces. In addition to the

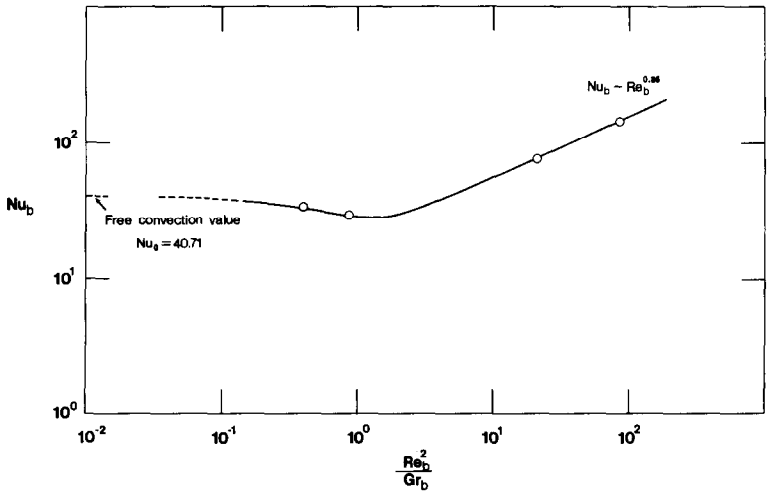

FIG. 7. Prediction of Nu_b vs Re_b^2/Gr_b for mixed convection flow in a heated cavity: $a/b = 1$, $\alpha = 45°$, $Gr_b = 4.4 \times 10^7$ and $\Delta T/T_\infty = 1.26$.

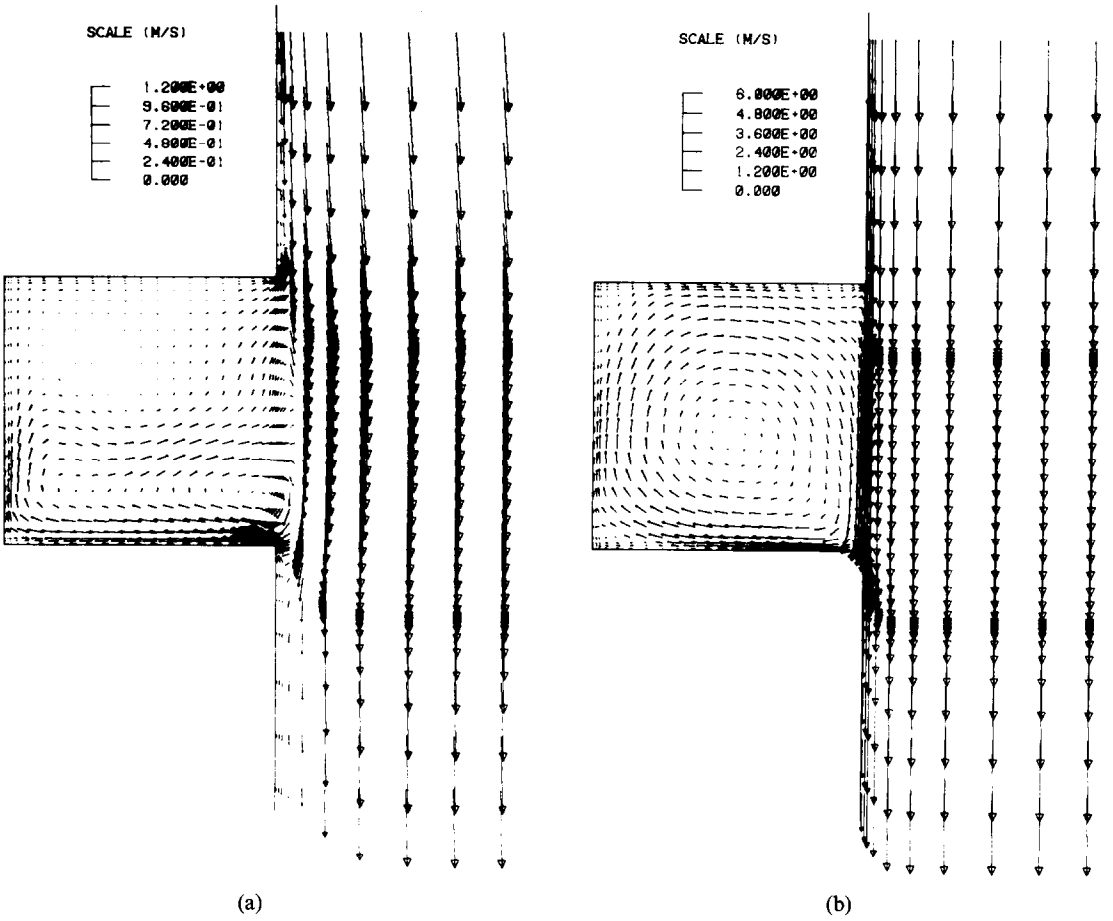

FIG. 8. Velocity vector plot for mixed convection flow in a heated cavity with $a/b = 1, \alpha = 45°, Gr_b = 4.4 \times 10^7$ and $\Delta T/T_\infty = 1.26$. From left to right $Re_b^2/Gr_b = 0.85$ and 21.3.

main rotating flow, small recirculation zones, or eddies, appear at both of the inner cavity corners. A tendency for a third eddy to form at the top aperture plane corner is also evident, but even at $Re_b^2/Gr_b = 85.4$ flow separation did not occur. These corner eddies are typical of wall-driven cavity flows; see, for example, [27], and both their size and intensity increased with increasing Re_b^2/Gr_b.

The corresponding temperature field in Fig. 9b shows the dominant influence of forced convection. Hot air is recirculated along the periphery of the cavity from which it escapes mainly through molecular and turbulent diffusion. Large levels of turbulent kinetic energy (plotted in ref. [21]) were observed in the cavity aperture plane where shearing production is intense. Part of this turbulence is convected into the cavity where it enhances the wall heat transfer, the remainder being driven downstream. High levels of the temperature fluctuations were also confined to the aperture plane and the cavity walls [21]. The magnitude of the temperature fluctuations was found to decrease with increasing Re_b^2/Gr_b, due to the higher degree of mixing of fluid in the cavity.

In closing this section we note that the approximations made to simulate the far field boundary conditions for the mixed convection cavity flows investigated by Humphrey *et al.* [2, 3] have yielded predicted flow patterns and temperature distributions that are in good qualitative agreement with their experimental observations [21].

4. CONCLUSIONS

The KEM formulation of Part I of this work was further extended to predict free and mixed convection flows in strongly heated, rectangular cavities of variable cross-section and orientation. Relatively good agreement is obtained between measurements and predictions of the mean velocity and temperature distributions in the free convection regime, but the turbulent kinetic energy and eddy diffusion coefficient are consistently underpredicted when $\alpha = 0°$. As a result, although the relative trends in predicted heat transfer, as a function of a/b and α, are in agreement with the available measurements, the Nusselt numbers differ significantly in their absolute values. Because of experimental uncertainties it is difficult to assess the accuracy of the heat transfer calculations. However, the

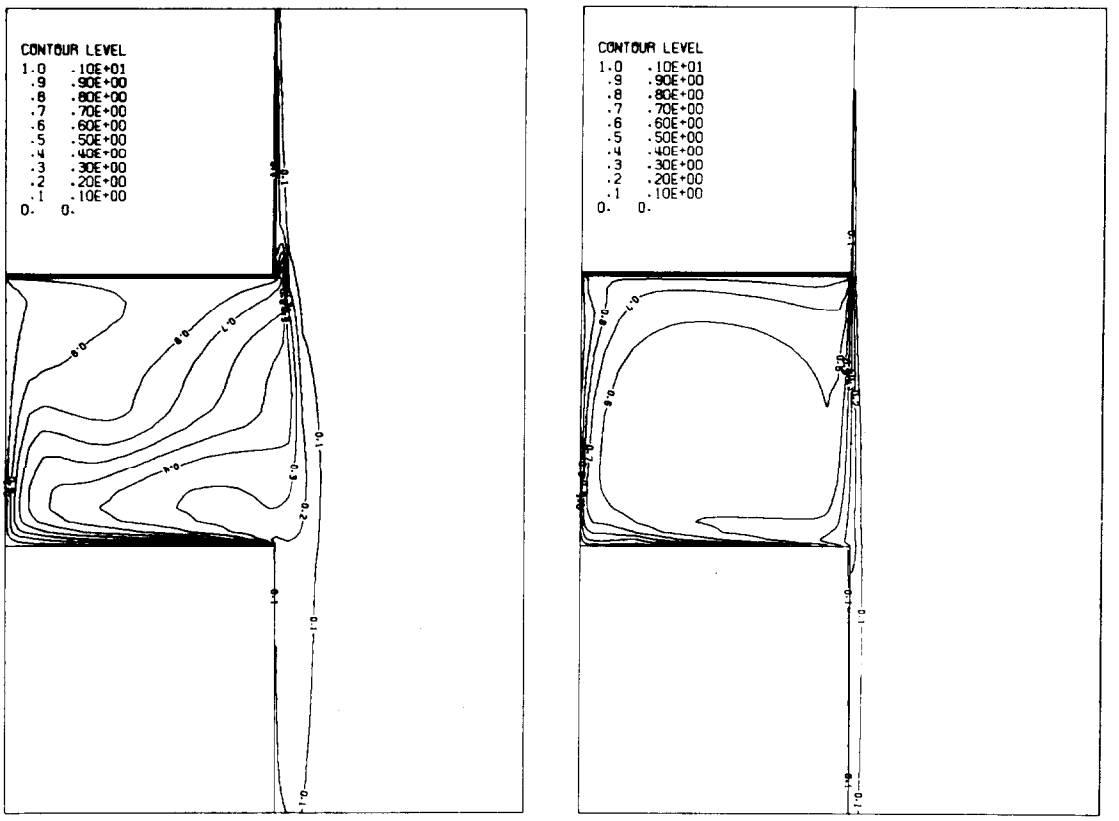

(a) (b)

FIG. 9. Contours of nondimensional temperature (θ) for mixed convection flow in a heated cavity with $a/b = 1$, $\alpha = 45°$, $Gr_b = 4.4 \times 10^7$ and $\Delta T/T_\infty = 1.26$. From left to right $Re_b^2/Gr_b = 0.85$ and 21.3.

uncertainties are such that, were it possible to adjust for their effects on the experimental data, this would significantly reduce the discrepancies between measurements and calculations of the heat transfer and turbulence quantities, particularly the turbulent kinetic energy.

The free convection calculations show that, regardless of orientation and aspect ratio, the cavity Nusselt number correlates well with $Gr_b^{1/3}$. A comparison between calculated 2-D and measured 3-D heat transfer coefficients supports the notion that 3-D motions strongly affect the heat transfer from the top and back walls in a cubical cavity.

Calculations of mixed convection in a cavity with $a/b = 1$ and $\alpha = 45°$ reveal a minimum in the Nusselt number for $Re_b^2/Gr_b = O(1)$. For $Re_b^2/Gr_b > 2$, the heat losses from a cavity are strongly influenced by inertial effects. By $Re_b^2/Gr_b > 21.3$ the flow field in a heated cavity is independent of orientation with respect to gravity and presents all the characteristics typical of a shear-driven cavity flow.

For both free and mixed convection, the predicted flow patterns are in good qualitative agreement with the flow visualization observations of Humphrey *et al.* [2, 3]. While their experiments confirm the assumption of turbulent flow for all the conditions investigated here, they do not rule out the possibility of a mean flow unsteadiness that was not detected. This could explain part of the discrepancy existing between measurements and calculations of the turbulent kinetic energy and heat transfer in free convection. This last point is the subject of continuing research.

Acknowledgements—Funding for this study was provided by Sandia National Laboratories, Livermore, through Contract No. 20–1012. We gratefully acknowledge this support and the keen interest shown in this work by our colleagues at Sandia. Our gratitude goes to Professor F. S. Sherman who provided many useful comments and constant encouragement throughout the entire investigation.

REFERENCES

1. D. D. Gray and A. Giorgini, The validity of the Boussinesq approximation for liquids and gases, *Int. J. Heat Mass Transfer* **19**, 545–551 (1976).
2. J. A. C. Humphrey, F. S. Sherman and K. Chen, Experimental study of free and mixed convective flow of air in a heated cavity, Contractor Report No. SAND84-8192, Sandia National Laboratories, Livermore, CA (1985).
3. K. S. Chen, J. A. C. Humphrey and F. S. Sherman, Free and mixed convective flow of air in a heated cavity of variable rectangular cross-section and orientation, *Phil. Trans. R. Soc.* **A316**, 57–84 (1985).

4. A. C. Ku, M. L. Doria and J. R. Lloyd, Numerical methods of unsteady buoyant flows generated by fire in a corridor, *16th Symposium. Int. Combustion Proc.*, Vol. 10, pp. 1373–1384 (1976).
5. N. C. Markatos, M. R. Malin and G. Cox, Mathematical modelling of buoyancy-induced smoke flow in enclosure, *Int. J. Heat Mass Transfer* **25**, 63–75 (1982).
6. S. Kumar and G. Cox, The application of numerical field model of smoke movement to the physical scaling of compartment fire. In *Numerical Methods in Thermal Problems* (edited by R. W. Lewis, J. A. Johnson and W. R. Smith), *Proc. 3rd National Conference*, Seatle, WA, pp. 837–848. Pineridge Press Swansea (1983).
7. W. P. Jones and B. E. Launder, The prediction of laminarization with a two-equation model of turbulence, *Int. J. Heat Mass Transfer* **15**, 301–314 (1972).
8. M. P. Fraikin, J. J. Portier and C. J. Fraikin, Application of a k–ε turbulence model to an enclosed buoyancy driven recirculating flow, ASME Paper No. 80-HT-68. Presented at the Joint ASME/AIChE National Heat Transfer Conference, Orlando, FL (July 1980).
9. K. Sagara, Calculation of turbulent gravity flow, *Trans. of the Architectural Institute of Japan*, No. 305, 88–96 (1981). Translated by Katsuhiro Asano, Department of Architecture, Faculty of Engineering, Nagoya University, Furocho, Chikusaku, Nagoya, Japan.
10. C. Hess and R. Henze, Experimental investigation of natural convection losses from open cavities, *J. Heat Transfer* **106**, 333–338 (1984).
11. F. Penot, Contribution a l'étude de la convection naturelle dans les espaces semi-confines. Ph.D. thesis, University of Poitiers, France (1981).
12. H. Mirenayat, Etude experimentale de transfert de chaleur par convection naturelle dans une cavité isotherme ouverte. Ph.D. thesis, University of Poitiers, France (1981).
13. J. S. Kraabel, An experimental investigation of natural convection from a side-facing cubical cavity, *ASME–JSME Thermal Engineering Joint Conference Proc.*, Vol. 1, pp. 299–306, Honolulu, HI, (March 1983).
14. P. LeQuere, J. A. C. Humphrey and F. S. Sherman, Numerical calculation of thermally driven two-dimensional unsteady laminar flow in cavities of rectangular cross section, *Numer. Heat Transfer* **4**, 249–283 (1981).
15. W. K. George and S. P. Capp, A theory for natural convection turbulent boundary layers next to heated vertical surfaces, *Int. J. Heat Mass Transfer* **22**, 813–826 (1979).
16. H. Tennekes and J. L. Lumley, *A First Course in Turbulence*. MIT Press, Cambridge, MA (1972).
17. V. Sernas and I. Kyriakides, Natural convection in an open cavity, *Proc. 7th Int. Heat Transfer Conference*, Munich, F.R.G. (1982).
18. J. Koseff, R. Street, P. Grecho, C. Upson, J. Humphrey and W. M. To, A three dimensional lid-driven cavity flow: experiment and simulation, *Proc. 3rd Int. Conference on Numerical Methods in Laminar and Turbulent Flow*, Seattle, WA (August 1983).
19. J. Fox, Heat transfer and air flow in transverse rectangular notch, *Int. J. Heat Mass Transfer* **8**, 269–279 (1965).
20. E. Chin, D. Rafiincjad and R. A. Seban, Prediction of the flow and heat transfer in a rectangular wall cavity with turbulent flow, *J. appl. Mech.* 351–358 (1972).
21. J. A. C. Humphrey, F. S. Sherman and W. M. To, Numerical simulation of buoyant turbulent flow, Contract Report No. SAND85-8180, Sandia National Laboratories, Livermore, CA (1985).
22. W. Rodi, Influence of buoyancy and rotation on equations for the turbulent length scale, *Proc. Second Symposium on Turbulent Shear Flows*, London, 10.37–10.42 (1979).
23. D. L. Siebers and J. S. Kraabel, Estimating convective energy losses from solar central receivers, Report SAND84-8717, Sandia National Laboratories, Livermore, CA (April 1984).
24. F. Pourahmadi and J. A. C. Humphrey, Prediction of curved channel flow with an extended k–ε model of turbulence, *AIAA Jl* **21**, 1365 (1983).
25. M. Ljuboja and W. Rodi, Prediction of horizontal and vertical turbulent buoyant wall jets, *J. Heat Transfer* **103**, 343–349 (1981).
26. R. L. Haugen and A. M. Dhanak, Heat transfer in turbulent boundary-layer separation over a surface cavity, *J. Heat Transfer* **89**, 335–340 (1967).
27. J. Koseff, Momentum transfer in a complex recirculating flow. Ph.D. thesis, Stanford University (1983).

SIMULATION NUMERIQUE D'UN ECOULEMENT TURBULENT LIBRE. II—CONVECTION NATURELLE ET MIXTE DANS UNE CAVITE CHAUFFEE

Résumé—Dans la première partie de l'étude deux modèles appliqués à la convection naturelle le long d'une plaque verticale chaude montrent des résultats précis pour l'écoulement moyen et le transfert thermique. Par suite, le plus simple des deux (une formulation k–ε basée sur la notion des diffusivités turbulentes de quantité de mouvement et de chaleur) est étendu à la prévision de la convection naturelle et mixte d'air dans une cavité de section rectangulaire avec une orientation quelconque. Ceci fait l'objet du présent texte. Les calculs numériques montrent que les détails de la convection naturelle sont fortement gouvernés par les caractéristiques du transfert thermique local. Celles-ci dépendent du rapport de forme a/b, de l'angle d'inclinaison α et du nombre de Grashof Gr_b. Par exemple, une stratification stable de fluide, dans une cavité inclinée, amortit fortement les fluctuations turbulentes, réduisant aussi les pertes thermiques de la cavité. Des calculs conduits pour les cas étudiés expérimentalement par Humphrey *et al.* [Sandia Report, No. SAND 84-8192 (1985); *Phil. Trans. R. Soc.* **A316**, 57–84 (1985)] montrent un bon accord qualitatif avec les distributions mesurées de vitesse et de température. Les prévisions du nombre de Nusselt, Nu, donnent des tendances qui sont aussi en accord avec les mesures. Pour la convection mixte, les détails de l'écoulement deviennent asymptotiquement indépendants de α quand le rapport des forces d'inertie aux forces d'Archimède, caractérisé par Re_b^2/Gr_b, augmente. Pour $a/b = 1$ et $\alpha = 45°$, les prévisons révèlent un minimum de Nu_b, quand $Re_b^2/Gr_b \sim 1$. La plupart des configurations complexes de l'écoulement observées expérimentalement sont reproduites numériquement, à la fois pour les convections naturelle et mixte.

NUMERISCHE SIMULATION TURBULENTER AUFTRIEBSSTRÖMUNGEN—II. FREIE UND GEMISCHTE KONVEKTION IN EINER BEHEIZTEN VERTIEFUNG

Zusammenfassung—Numerische Berechnungen zeigen, daß die freie Konvektionsströmung in einer beheizten Vertiefung stark durch den örtlichen Wärmeübergang bestimmt wird. Die Charakteristik hängt vom Seitenverhältnis a/b der rechteckigen Vertiefung, vom Neigungswinkel α und von der Grashof-Zahl Gr_b ab. Eine stabile Schichtung des beheizten Fluides in einer geneigten Vertiefung dämpft beispielsweise die turbulenten Bewegungen stark und reduziert auf diese Weise die konvektiven Wärmeverluste. Berechnungen, welche für die von Humphrey und anderen experimentell untersuchten Fälle der freien Konvektion ausgeführt worden sind, zeigen eine qualitativ gute Übereinstimmung mit den gemessenen Geschwindigkeits- und Temperaturverteilungen. Die vorausberechneten Nusseltzahlen, Nu_b, stimmen ebenfalls qualitativ mit den Messungen überein. Für gemischte Konvektion hängt die Strömung umso weniger von α ab, je größer das Verhältnis von Trägheits- zu Auftriebskräften, charakterisiert durch Re_b^2/Gr_b ist. Für $a/b = 1$ und $\alpha = 45°$ zeigen die Vorhersagen ein Minimum für die Nusseltzahl, Nu_b, wenn $Re_b^2/Gr_b \approx 1$. Viele der komplexen Strömungsmuster, die experimentell für freie und gemischte Konvektion gefunden wurden, sind numerisch reproduziert worden.

ЧИСЛЕННОЕ ИССЛЕДОВАНИЕ ПОДЪЕМНОГО ТУРБУЛЕНТНОГО ТЕЧЕНИЯ—II. СВОБОДНАЯ И СМЕШАННАЯ КОНВЕКЦИЯ В НАГРЕТОЙ ПОЛОСТИ

Аннотация—В первой части работы предложены две модели расчета свободно-и смешанноконвективных турбулентных потоков с малыми числами Рейнольдса. Сравнение данных измерений и расчетов для свободной конвекции у нагретой вертикальной плоской пластины показали, что обе модели дают точные результаты для средних значений характеристик потока и теплопереноса. Более простая из двух моделей (k–ε-модель, основанная на понятии турбулентной температуропроводности для импульса и тепла) применена для расчета устойчивых свободно-и смешанноконвективных потоков воздуха в сильно нагретой полости произвольных прямоугольного сечения и ориентации. Численные результаты показывают, что на отдельные участки свободноконвективного потока сильное влияние оказывает локальный теплоперенос, характеристики которого зависят от отношения сторон полости a/b, угла наклона α и числа Грасгофа Gr_b. Например, устойчивая стратификация нагретой жидкости внутри наклонной полости сильно подавляет турбулентные флуктуации, уменьшая таким образом конвективные потери тепла из полости. Расчеты, проведенные Хампреем и др. [Sandia Report No. SAND 84-8192 (1985); *Phil. Trans. R. Soc.* **A316**, 57 (1985)], показали хорошее качественное совпадение численных данных с измерениями распределений скорости и температуры, числа Нуссельта Nu_b. Для смешанной конвекции структура потока становится асимптотически независимой от α, поскольку отношение инерционных и подъемных сил, характеризуемое Re_b^2/Gr_b, растет. Для $a/b = 1$ и $\alpha = 45°$ рассчитано минимальное значение Nu_b при $Re_b^2/Gr_b \sim 1$. Приводится много примеров численного исследования сложных течений.